Eng Int Syst (2023) 5: 395–401

Engineering
Intelligent Systems

Power Conversion Technology of Power Electronics Equipment Based on SiC Conversion Circuit

Xiaoyu Yang* and Hui Liu

Electrical Engineering Department, Zhengzhou Railway Vocational and Technical College, Zhengzhou 451460, China

In order to achieve the power conversion of power electronics equipment and eliminate the over-voltage peak phenomenon during the conversion process, a SiC conversion circuit is designed and applied to the power conversion process. As the power switches of power electronics transformers, SiC devices are frequently applied in isolated bidirectional DC/DC converter units to form SiC converter circuits. Given the phenomenon of double-active bridge in a SiC converter circuit, the double-active full bridge phase shift control mode was selected; that is, the driving signals on both sides of H-bridge were controlled by phase differences to convert the different operation states of the SiC converter circuit in one operation cycle to complete the power conversion. The results show that by maximizing the turn-off resistance, the turn-off peak of FET can be reduced, the interference between electromagnetic wave and power electronic components can be alleviated, and the turn-off safety of FET can be ensured. By determining the angle difference of trigger pulse of different switches, the voltage on both sides of H-bridge can be obtained to achieve power transfer and conversion.

Keywords: SiC; conversion circuit; power electronics equipment; electric energy conversion; double-active bridge; inductive current.

1. INTRODUCTION

With the general development nowadays of technologies for power systems, power electronics equipment that can achieve isolation, voltage conversion and power flow control has attracted an increasing amount of attention, and is widely used in many fields such as the smart grid and energy internet [1, 2]. Given the low power semiconductor technology, which leads to limited capacity to withstand the voltage performance of the semiconductor, the topology structure constructed by multiple power sub-modules is widely used in current power electronics equipment [3].

Compared with the insulated gate bipolar transistor [4], the silicon FET has several significant advantages including high switching frequency, ability to withstand high voltage, and low switching loss [5], which can effectively improve the performance of power electronics transformers. On the other hand, the devices made of SiC (silicon carbide) have the advantages of low on-resistance and high working temperature because of the features of silicon FET [6]. They are mainly used in the power conversion applications of power electronics equipment. Based on this research, the power conversion technology of power electronics equipment based on SiC conversion circuit meets the requirements of power electronics equipment for high temperature, high voltage resistance and low loss.

*Email of corresponding author: yangxiaoyu@mjc-edu.cn

2. ELECTRIC ENERGY CONVERSION TECHNOLOGY OF POWER ELECTRONIC EQUIPMENT

2.1 Power Electronics Transformer Based on SiC Conversion Circuit

To realize the electric energy conversion of power electronics equipment, the SiC device, as the power switch of power electronics transformer, is applied to the high-frequency

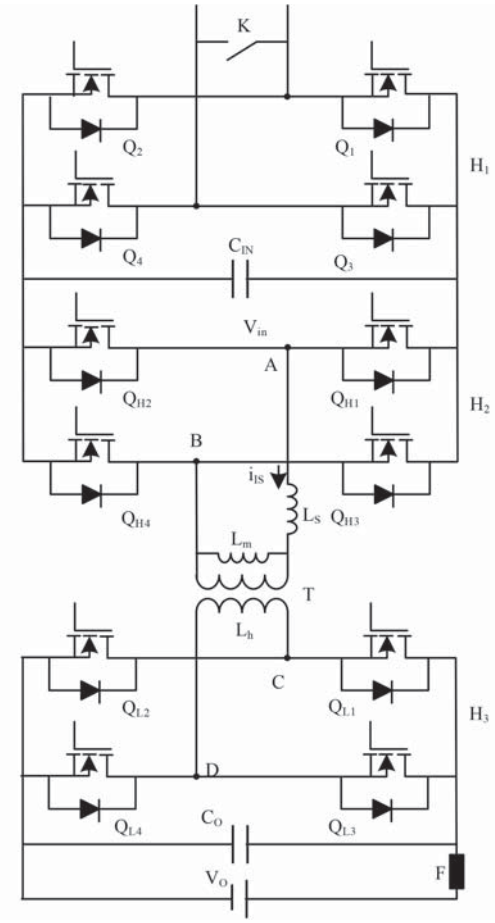

Figure 1 Topology diagram of the SiC conversion circuit.

isolated bidirectional DC/DC converter to form the SiC conversion circuit, thus giving full play to the interface circuit function of the DC battery unit [7]. The chain multilevel converter is used as the power grid access circuit on the AC side [8], and the common DC bus is constructed by means of the SiC conversion circuit to form the power electronics energy storage PCS device. Figure 1 shows the topological structure of the SiC conversion circuit.

In Figure 1, the H_1 unit contains a power factor correction circuit switch tube whose main function is to correct the voltage of the input capacitor C_{IN} with an appropriate modulation index, which can be described by Q_1–Q_4; Unit H_2 and Unit H_3 respectively contain high-voltage side and low-voltage side switch tubes of double active bridge circuits, which are respectively described as Q_{H1}–Q_{H4} and Q_{L1}–$Q_{L4}0$. K, T, F respectively represent the sub-module bypass switch, high-voltage isolation high-frequency transformer and output fuse protection fuse; C_o, L_s and L_m represent the output capacitance, the phase-shift inductance and the excitation inductance of T, respectively.

$M = 1{:}1$ represents the primary-secondary ratio of T, and the input and output voltages of the double active bridge circuit are consistent. The formula is described as follows:

$$V_m = V_o = U_o \tag{1}$$

V_{AB} and V_{CD} represent the voltage difference between point A and point B and between point C and point D, respectively. Considering $L_m \gg L_S$, the double-active bridge circuit in the SiC conversion circuit can be simplified without considering L_m. In the simplified double active bridge circuit, θ can be used to represent the phase angle difference between V_{AB} and V_{CD}, that is, the phase shift angle.

2.2 Control of SiC Conversion Circuit

Generally, the pulse width modulation control mode is selected for SiC conversion circuit [9]. Because the double-active bridge circuit is used in the SiC conversion circuit, the double-active full-bridge phase shift control mode is adopted to flexibly control the conversion of power and energy of the circuit.

Figure 2 shows the operation waveform diagram of SiC converter circuit under double-active full-bridge phase shift control mode, in which the trigger pulses of high-voltage side and low-voltage side switches of double active bridge circuit in H_2 unit and H_3 unit are denoted by $G_{1–4}$ and $g_{5–8}$ respectively.

There are ten different operating states in one operating cycle of the SiC conversion circuit [10].

(1) The first state

At time t_0, the SiC conversion circuit is generally in a stable state, that is, $L_m = U_A$ and $L_h = U_B$. And the inductive current is fixed. The fluctuation rate of the inductive current $\frac{di}{dt}$ is described by Formula (2):

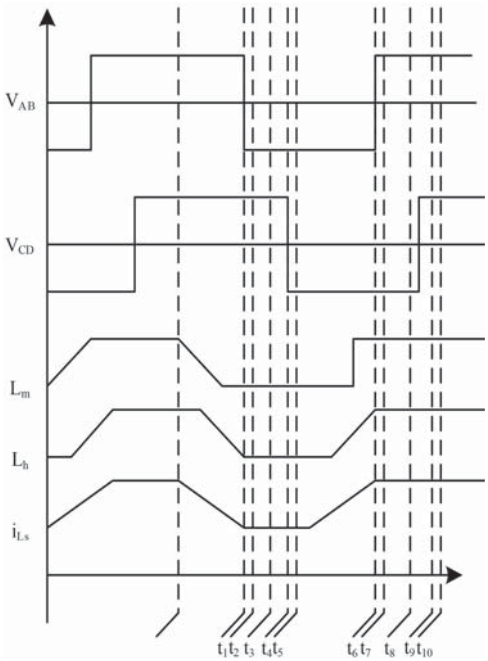

Figure 2 Waveform diagram under double-active full-bridge phase shift control mode.

$$\frac{di}{dt} = 0 \tag{2}$$

(2) The second state

At time t_1, Q_{H1} and Q_{H4} switches in H_2 unit are turned off. Considering the influence of capacitors C_{H1} and C_{H4}, Q_{H1} and Q_{H4} switches meet the zero-voltage turn-off condition [11]. In this case, the H_2 unit discharges through the capacitors Q_{H4} and C_{H3}. Moreover, considering the influence that the inductive current cannot suddenly change [12], it is formed by freewheel diodes. The fluctuation rate $\frac{di}{dt}$ of the inductive current in this state can be expressed by Formula (3):

$$\frac{di}{dt} = \frac{U_B - (U_A - V_{CH1} - V_{CH4})}{L} \tag{3}$$

(3) The third state

At time t_2, considering the effect of freewheel diodes D_{H2} and D_{H3} in H_2 unit, the switches in Q_{H2} and Q_{H3} meet the zero voltage conduction condition [13]. Under this condition, the left bridge of the converter $L_m = U_A$ and $L_h = U_B$, and the inductive current decreases continuously. The fluctuation rate $\frac{di}{dt}$ of inductive current in this state can be expressed by Formula (4):

$$\frac{di}{dt} = \frac{U_B + U_A}{L} \tag{4}$$

(4) The fourth state

At time t_3, according to the above theoretical description, considering the role of freewheel diodes D_{L2} and D_{L3} in H_3 cell, Q_{L1} and Q_{H4} meet the zero voltage conduction condition, and capacitors C_{L1}, C_{L4}, C_{L2} and C_{L3} discharge and are charged respectively. Under this condition, the inductive current will cross 0, and at the same time, the commutation motion is carried out [14]. The fluctuation rate $\frac{di}{dt}$ of the inductive current in this state can be expressed by Formula (5):

$$\frac{di}{dt} = -\frac{U_B + U_A}{L} \tag{5}$$

(5) The fifth state

At time t_4, the Q_{L1} and Q_{L4} switches in the H_3 cell are in the 'off' state. Taking into account the influence of capacitors C_{L1} and C_{L4}, Q_{L1} and Q_{L4} meet the zero-voltage turn-off standard. Under this condition, capacitors C_{L2} and C_{L3} in H_3 cell discharge. Moreover, as the inductive current cannot suddenly change, it is formed by freewheel diodes D_{L2} and D_{L3}. The fluctuation rate $\frac{di}{dt}$ of inductive current in this state can be expressed by Formula (6):

$$\frac{di}{dt} = -\frac{U_A + (U_B - V_{CL1} - V_{CL4})}{L} \tag{6}$$

(6) The sixth state

At time t_5, Q_{H2} and Q_{H3} in H_2 unit, freewheel diodes D_{H2} and D_{H3} form a conduction loop with the power supplies on both sides, thus causing the inductive current to continuously increase in the opposite direction [15]. The fluctuation rate $\frac{di}{dt}$ of inductive current in this state can be expressed by Formula (7):

$$\frac{di}{dt} = \frac{U_B - U_A}{L} \tag{7}$$

(7) The seventh state

At time t_6, the Q_{H2} and Q_{H3} switches in H_2 unit are turned off. Considering the influence of capacitors C_{H2} and C_{H3}, Q_{H2} and Q_{H3} meet the zero-voltage turn-off

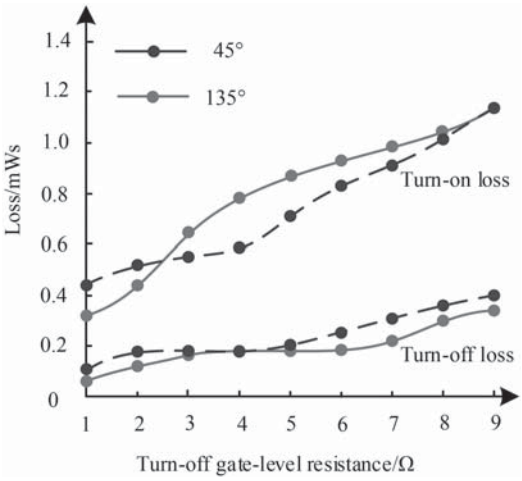

Figure 3 Curve of sic conversion circuit loss and gate-level resistance.

standard. Under this condition, capacitors C_{H1} and C_{H4} in H_2 cell discharge. Since the inductive current cannot suddenly change, it is formed by freewheel diodes D_{H1} and D_{H4}. The fluctuation rate $\frac{di}{dt}$ of inductive current in this state can be expressed by Formula (6):

$$\frac{di}{dt} = -\frac{U_B - (U_A - V_{CH2} - V_{CH3})}{L} \tag{8}$$

(8) The eighth state

At time t_7, considering the effect of D_{H1} and D_{H4}, the switches Q_{H1} and Q_{H4} in H_2 unit are turned on at zero voltage, resulting in the left bridge of the converter $L_m = U_A$ and the continuous decrease of inductive current. The fluctuation rate $\frac{di}{dt}$ of inductive current in this state can be expressed by Formula (9):

$$\frac{di}{dt} = \frac{U_B + U_A}{L} \tag{9}$$

(9) The ninth state

At time t_8, Q_{L2} and Q_{L3} switches in H_3 unit are in a 0-current conducting state. And capacitors C_{L2}, C_{L3}, and C_{L1}, C_{L4} discharge and are charged respectively. Under this condition, the inductive current is 0. Meanwhile, the commutation motion is carried out. The fluctuation rate $\frac{di}{dt}$ of inductive current in this state can be expressed by Formula (10):

$$\frac{di}{dt} = \frac{U_B + U_A}{L} \tag{10}$$

(10) The 10th state

At time t_9, Q_{L2} and Q_{L3} switches in H_3 unit are turned off. Considering the effects of capacitors C_{L2} and C_{L3}, Q_{L2} and Q_{L3} meet the zero-voltage turn-off standard. Under this condition, capacitors C_{L1} and C_{L4} in H_3 cell discharge. Since the inductive current cannot suddenly change, it is formed by D_{L1} and D_{L4}. The fluctuation rate $\frac{di}{dt}$ of inductive current in this state can be expressed by Formula (11):

$$\frac{di}{dt} = \frac{U_A - (U_B - V_{CL1} - V_{CL4})}{L} \tag{11}$$

When the state of the SiC conversion circuit reaches t_{10}, it can return to the first state (i.e., t_0), and the cycle is repeated to complete the electric energy conversion of the power electronics equipment.

3. CASE ANALYSIS

To test the application effect of power electronic equipment power conversion technology based on SiC conversion circuit in power conversion of actual power electronic equipment, a specific type of converter was selected as the application object, and its power was converted by the proposed technology. The performance of this technology was verified by experimental tests.

3.1 Dual Pulse and Short Circuit Test

In order to apply and test the proposed technology, dual pulse test platform was built, and the switching loss incurred when the technology was applied was evaluated.

Because the FET used in this technology involved a hard turn-off, it was necessary to ensure the turn-off safety margin of the SiC converter circuit in the practical application of this technology. Figure 3 shows the curve of loss and gate-level resistance of SiC conversion circuit.

As shown in Figure 3, when the turn-off gate-level resistance increases gradually, the turn-off loss of incurred by the proposed technology increases slowly, which is obviously different from the rapid development trend of turn-on loss. Therefore, in order to improve the overall efficiency, reduce the turn-off peak of FET, alleviate the interference between electromagnetic waves and power electronic components, and ensure the turn-off safety margin of FET, it is necessary to maximize the turn-off resistance.

By means of dual pulse detection, the switching loss, voltage and current volatility of this technology can be determined. Based on the dual pulse detection platform that was constructed, the technology proposed in this paper was tested. The results are shown in Table 1 and Figure 3.

Table 1 Dual pulse test data.

Parameter	Test value
Rated current/A	48
Turn-on/V·ns^{-1}	11
Turn-off/A·ns^{-1}	2
Gate-level turn-off resistance/Ω	9
Gate-level capacitance/nF	2.1
Turn-on loss/mJ	1.87
Turn-off loss/mJ	0.98
Pole-on resistance/Ω	4.6
Bus voltage/V	739
Rated current turn-off peak/V	857

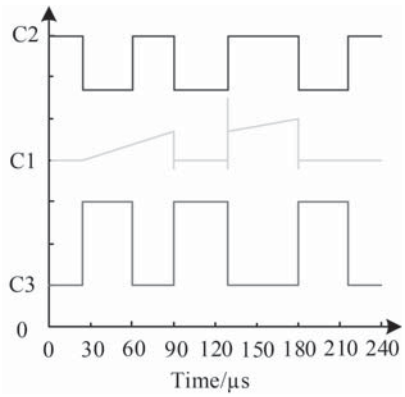

Figure 4 Dual pulse test waveform.

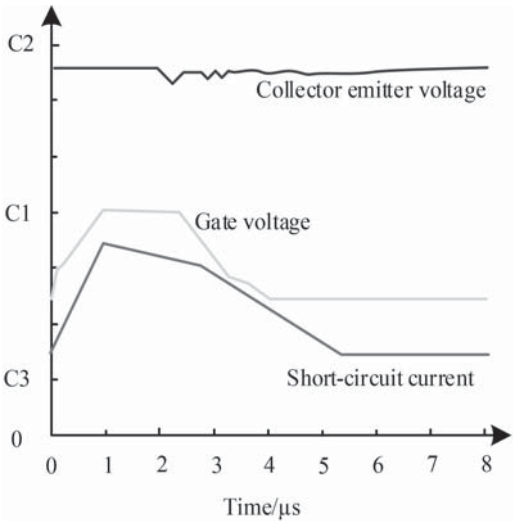

Figure 5 Short-circuit waveform.

Based on the results of the dual pulse test shown in Table 1 and Figure 4, combined with the on-state resistance value of SiC converter circuit in this technology, the overall loss P_M of all power devices of the double active bridge circuit under the condition of soft turn-on of zero voltage switching can be roughly determined:

$$P_M = P_{on} + P_{off} \tag{12}$$

In Formula (12), P_{on} and P_{off} represent the overall on-state loss and the overall off-state loss of the SiC conversion circuit respectively.

The calculation based on Formula (12) shows that the overall loss of SiC conversion circuit in this technology is 210.4W.

When the short-circuit current value is given, under the corresponding working conditions, the short-circuit current peak value can be obtained through a short-circuit test. Figure 5 shows the short-circuit waveform after the application of this technology.

As shown in Figure 5, the time from the gate pole turn-on to the start of the gate pole turn-off is about 1.5 μs, which can meet the standard of the detection time for driving-circuit

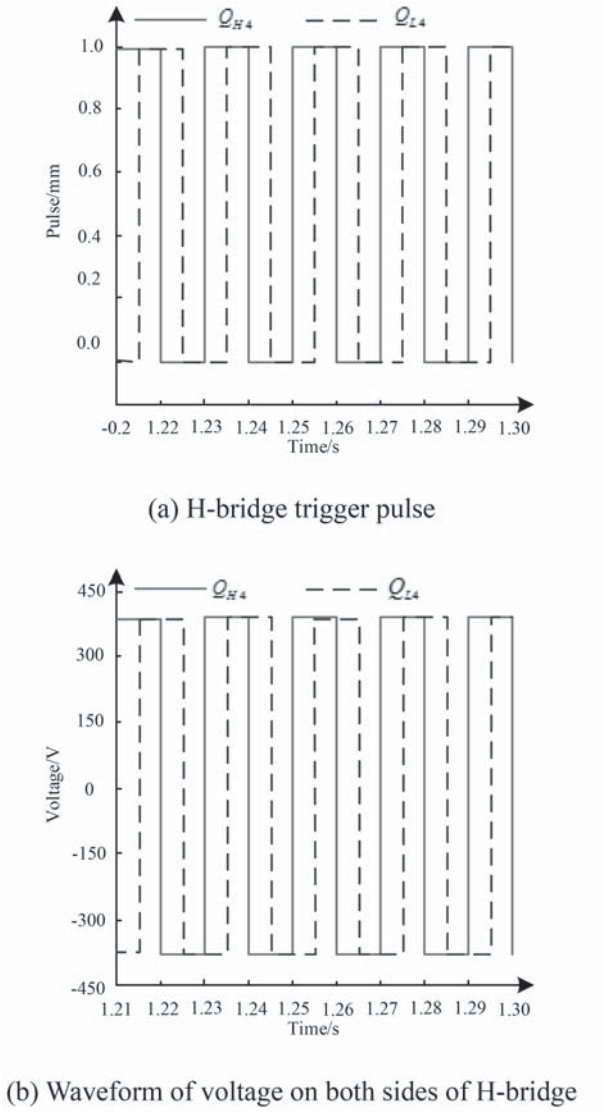

Figure 6 Test results of power transfer.

protection. The overvoltage peak phenomenon is obviously improved by the fault soft turn-off, and there is basically no overvoltage peak phenomenon in the short-circuit current.

3.2 Power Transfer Test

For the purpose of testing the working state and power transfer process of the technology proposed in this paper, the power transfer test was carried out after setting the relevant operating parameters. The results are shown in Figure 6.

Figure 6(a) shows the trigger pulses of Q_{H4} and Q_{L4} on the left side of the H-bridge. Analysis shows that the trigger pulse of Q_{L4} leads/lags behind the trigger pulse of Q_{H4} by a certain angle. According to Figure 6(b), there is a certain phase difference between the voltages on both sides of the H-bridge. Therefore, this indicates that the technology proposed in this paper can meet the control requirements for the degree of freedom of the phase shift angle, and the voltage on both sides of the H-bridge can be obtained by determining the angle difference of the trigger pulse of different switching tubes, so as to complete the power transmission and conversion.

4. CONCLUSION

In this paper, the power conversion technology of power electronic equipment based on SiC conversion circuit is studied, and the SiC conversion circuit is applied to the power electronic transformer. The experimental results show that the technology proposed in this paper can achieve the purpose of power transmission and conversion.

REFERENCES

1. Lei WJ, Liu JJ, Lu GT, et al. 2020. Overview of comprehensive analysis and evaluation methods for reliability of key components and systems of large-capacity power electronic equipment. *High Voltage Engineering, 46*(10): 3353–3361.
2. He XN, Wang RC, Wu JD, et al. 2020. Information characteristics of power electronic transformation and information control technology from discrete digitalization of electric energy to intelligence. *Proceedings of the CSEE, 40*(5): 5–6.
3. Huangfu HW, Zhang XY. 2020. Rectification oscillation suppression of ISOP phase-shifted full bridge converter based

on SiC devices. *Power Electronics Technology, 336*(11): 95–98.
4. Mo YB, Qin HH, Xiu Q, et al. 2020. Analysis of switching process of typical dual-supply RC driver circuit based on SiC BJT and realization of optimal loss. *Advanced Technology of Electrical Engineering and Energy, 39*(2): 30–39.
5. Hu WT, Shu ZL, Meng LH. 2019. Double active DC/DC converter based on minimum current effective value control. *Power Electronics, 53*(8): 99–102.
6. Ning PQ, Li L, Cao H, et al. 2018. Overview of hybrid switching devices based on Si IGBT/SiC MOSFET. *Advanced Technology of Electrical Engineering and Energy, 37*(10): 4–12.
7. Zhao Z, See KY, Wang W, et al. 2019. Voltage-dependent capacitance extraction of SiC power mosfets using inductively coupled in-circuit impedance measurement technique. *IEEE Transactions on Electromagnetic Compatibility, 61*(4): 1322–1328.
8. Guo B, Zhang YM, Zhang JL, et al. 2018. Hybrid control strategy of phase-shifted full bridge LLC converter based on direct phase shift angle control. *Transactions of China Electrotechnical Society, 33*(19): 169–179.
9. Wang ZG, Zheng KY, Zhang WG, et al. 2020. Design of isolated DC-DC converter driver circuit based on GaN HEMT. *Power Technology, 360*(9): 132–136.
10. Zeng JH, Sun ZF, Lei M, et al. 2019. Current-sharing control of independent input and parallel output double active full bridge DC-DC converter without current sensor. *Proceedings of the CSEE, 39*(7): 2144–2154.
11. Ando Y, Oku T, Yasuda M, et al. 2018. A compact SiC photovoltaic inverter with maximum power point tracking function. *Solar Energy, 141*: 228–235.
12. Feng ZQ, Chi S. 2019. Extended dual phase shift control for phase shift optimization of bidirectional full bridge DC/DC converter. *Electric Drive, 49*(7): 25–31.
13. Sun XT, Li J, Wang QB. 2018. Research and implementation of optimal control of bidirectional full bridge DC–DC converter. *Chinese Journal of Electronic Devices, 41*(5): 1159–1162.
14. Zhang HY, Shi ZT, Zhang ZF, et al. 2019. Research on constant current control of double active full bridge phase-shifted DC/DC converter. *Power Electronics, 53*(1): 104–106.
15. Jin L, Liu BY, Duan SX. 2018. Phase shift control of minimum return power of three-level double active full bridge DC-DC converter. *Transactions of China Electrotechnical Society, 33*(24): 5864–5873.